Asian Journal of Chemistry; Vol. 35, No. 12 (2023), 2929-2938

ASIAN JOURNAL OF CHEMISTRY

https://doi.org/10.14233/ajchem.2023.28278

Study of Bi-functional Applications of ZnO Nanoparticles Synthesized *via* Sonochemical Route

D.A. RAGHUPATHY[1,2], G. RAMGOPAL[3,*], V.G. DILEEP KUMAR[4,5], T. NAVEEN KUMAR[6] and C.R. RAVIKUMAR[7,*]

[1]Department of Physics, Dr. Ambedkar Institute of Technology, Bangalore-560056, India
[2]Department of Physics, Bharathiar University, Coimbatore-641046, India
[3]Department of Physics, Maharani's Science College for Women, Maharani Cluster University, Bengaluru-560001, India
[4]Department of Chemistry, HKBK College of Engineering, Bangalore-560045, India
[5]Department of Chemistry, PES University, 100 ft. Ring Road, BSK 3rd Stage, Bangalore-560085, India
[6]Department of P.G. Chemistry, Surana College, Autonomous Institute, Bangalore-560004, India
[7]Research Center, Department of Science, East West Institute of Technology (Affiliated to Visvesvaraya Technological University, Bangalore), India

*Corresponding authors: E-mail: dr_gramgopal@yahoo.co.in; ravicr128@gmail.com

Received: 30 July 2023; *Accepted*: 23 September 2023; *Published online*: 2 December 2023; AJC-21452

The sonochemical synthesis involved the dispersion of zinc oxide (ZnO) precursor in a suitable solvent, followed by ultrasonic irradiation to induce chemical reactions and nucleation of ZnO nanoparticles. The resulting nanomaterials exhibited a uniform particle size distribution, which is crucial for their photocatalytic efficiency. ZnO nanoparticles with a uniform particle size of 25 nm were successfully synthesized using a sonochemical route and were employed for the degradation of direct green and fast orange dyes under UV light irradiation. The band gap of the ZnO nanoparticles was determined to be 3.35 eV, indicating its potential as a photocatalyst for dye degradation. The degradation efficiency of the dyes was evaluated by monitoring the change in their concentration over time. The ZnO nanoparticles demonstrated excellent photocatalytic activity, efficiently degrading both dyes within a relatively short duration. The electrochemical studies further confirmed the potential applicability of the synthesized ZnO nanoparticles in various electrochemical systems. The ZnO electrode that was produced could detect lead in an acidic solution. The ZnO electrode is a promising electrode material for making sensor applications because of its higher electrochemical behaviour. Overall, this research contributes to the development of efficient and environmentally friendly approaches for wastewater treatment and lead sensor.

Keywords: ZnO nanoparticles, Sonochemical method, Photocatalytic activity, Cyclic voltammetry, Lead sensor.

INTRODUCTION

Zinc oxide (ZnO) nanoparticles have gained considerable attention in recent years due to their exceptional properties and diverse applications [1]. ZnO, a versatile semiconductor material, exhibits excellent optical, electrical and catalytic properties, making it suitable for various environmental and technological applications. One such application is the degradation of dyes, which are a major class of organic pollutants in wastewater [2]. The synthesis of ZnO nanoparticles has been extensively studied and various methods have been employed to obtain nanoparticles with desired properties. Among these methods, the sonochemical route has gained considerable popularity due to its simplicity, cost-effectiveness and ability to produce nanoparticles with uniform size and morphology. Sonochemistry involves the use of high-frequency sound waves to induce chemical reactions and promote the formation of nanomaterials [3].

The degradation of dyes using ZnO nanoparticles has emerged as a promising approach for wastewater treatment. Dyes, commonly used in industries such as textiles, printing and paper manufacturing, are known to be persistent and toxic to the environment. Traditional dye removal techniques often face limitations such as high cost, low efficiency and secondary pollution. Therefore, the development of efficient and eco-friendly methods for dye degradation is of great importance [4]. ZnO nanoparticles offer several advantages for dye degradation. First, their wide band gap enables efficient absorption

of UV light, which can be used to activate the photocatalytic properties of ZnO. Under UV light irradiation, ZnO nanoparticles generate reactive oxygen species (ROS) such as hydroxyl radicals (•OH), which exhibit strong oxidative properties and can effectively degrade organic dyes into harmless products. Additionally, ZnO nanoparticles possess a large surface area-to-volume ratio, providing abundant active sites for dye adsorption and catalytic reactions [5-7].

In addition to their photocatalytic activity, ZnO nanoparticles have been investigated through electrochemical studies to understand their electrochemical behaviour and potential applications in various electrochemical systems [8]. These studies involve evaluating the charge transfer processes occurring at the surface of ZnO nanoparticles, including the redox reactions and electron transfer kinetics. In this context, this study aims to synthesize ZnO nanoparticles *via* the sonochemical route and investigate their applications in the degradation of dyes under UV light irradiation. The uniform particle size and band gap of the synthesized ZnO nanoparticles will be characterized, along with their electrochemical properties. The findings from this study will contribute to advancing the understanding of ZnO nanoparticles and their potential utilization in environmentally friendly dye degradation and electrochemical applications.

EXPERIMENTAL

Synthesis of ZnO nanoparticles (ZnO NPs)**:** The probe sonication technique was utilized to synthesize ZnO NPs from the precursors zinc nitrate and sodium hydroxide. In brief, ZnO NPs was synthesized by adding a 0.5 M solution of NaOH dropwise to a 1 M solution of zinc nitrate in a 205 mL beaker and persistently stirring the mixture until precipitation was achieved. The solution was further sonicated using an ultrasonic pulse of 30 ± 2 kHz for about 1 h at 45 ºC which results in the formation of a white gelatinous precipitate. The obtained precipitate was subjected to thorough washing with distilled water to remove any impurities or residual reactants. Following the washing step, the precipitate was subjected to calcination at a temperature of 600 ºC.

$$Zn(NO_3)_4 + 4NaOH \longrightarrow Zn(OH)_4\downarrow + 4NaNO_3 \quad (1)$$

$$Zn(OH)_4 \longrightarrow ZnO(OH)_2\downarrow + H_2O \quad (2)$$

$$Zn(OH)_2 \longrightarrow ZnO + H_2O \quad (3)$$

Characterization: The crystalline nature and phase structure of ZnO NPs were investigated by XRD spectrometer-Shimadzu PXRD-7000 X-ray diffractometer with Cu*K*α radiation (λ = 1.541 Å). FTIR analyses of the sample were carried out using a Perkin-Elmer Spectrum-1000 FTIR spectrophotometer with KBr pellets in 4000-400 cm^{-1} region. The Elico SL-150 UV-vis spectrophotometer with a range of 200-800 nm was used to study the sample's optical properties and to study the degradation. The cyclic voltammetry measurement was performed using a three-electrode setup with a carbon paste electrode mixed with ZnO as the working electrode, platinum wire and Ag/AgCl as counter and reference electrodes, respectively and a 0.1 N HCl solution as electrolyte on an electrochemical analyzer (CHI608E potentiostat).

Fabrication of working electrode: For the fabrication of the working electrode graphite powder, silicon oil and synthesized ZnO nanoparticles in the ratio of 70:15:15 was manually ground using an agate mortar for around 30 min. A handmade Teflon cavity tube was then filled with the resulting paste. On a piece of weighing paper, the packed carbon paste's surface was smoothed [9].

RESULTS AND DISCUSSION

P-XRD studies: In Fig. 1, the PXRD pattern of the ZnO nanoparticles would typically display a series of diffraction peaks. The peaks in the diffraction pattern correspond to the crystal planes of the ZnO nanoparticles. The positions and intensities of the diffraction peaks were compared with the JCPDS card no. 89-1397 for ZnO [10]. The analysis revealed that the experimental peaks were in excellent agreement with the reference pattern, indicating the successful synthesis of ZnO nanoparticles with a wurtzite crystal structure. The average crystallite size (D) of the ZnO nanoparticles was estimated to be 25 nm by analyzing the line broadening observed in the X-ray diffraction spectra using Scherrer's formula. This size determination provides valuable information about the dimensions of the ZnO nanoparticles and confirms their nanoscale nature.

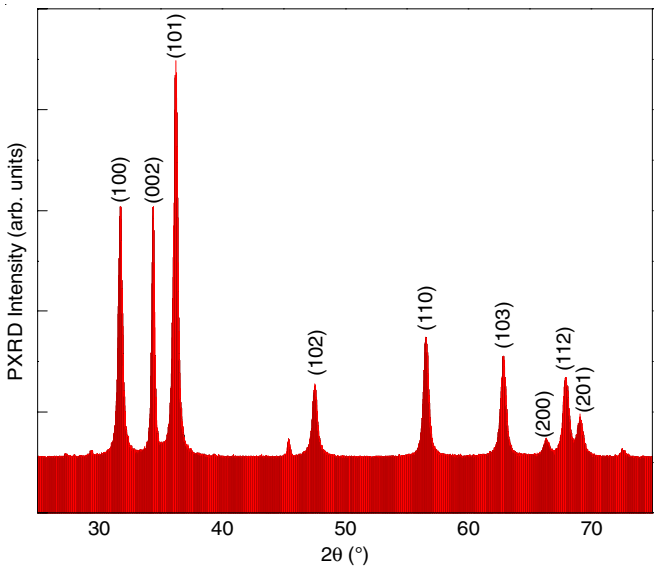

Fig. 1. PXRD Patterns of ZnO nanoparticles

$$D = \frac{K\lambda}{\beta\cos\theta} \quad (1)$$

The crystal lattice parameters of the synthesized ZnO nanoparticles were determined using eqn. 2 [11]:

$$\frac{1}{d^2} = \frac{4}{3}\left(\frac{h^2 + kh + l^2}{a^2}\right) + \frac{l^2}{c^2} \quad (2)$$

The obtained PXRD analysis results for ZnO nanoparticles synthesized through the sonochemical method are presented in Table-1. The table includes the Miller indices (*h k l*) corresponding to each diffraction peak, the interplanar spacing (*d*-spacing) calculated using the Bragg's equation, the

TABLE-1
FWHM VALUES, CRYSTALLITE SIZES, *d*-SPACING AND MILLER INDICES FOR ZnO NANOPARTICLES

2θ (°)	FWHM (°)	Crystallite size (nm)	d-spacing	Miller indices (hkl)
31.7718	0.52570	21.00	2.77416	100
34.4284	0.47840	18.74	2.51285	002
36.2487	0.39180	20.78	2.37621	101
47.5427	0.58790	16.93	1.81100	102
56.5926	0.50070	18.81	1.52500	110
2.8538	0.71720	17.65	1.35734	103
67.9535	0.74930	16.30	1.26835	112
69.1215	0.64660	19.32	1.23788	201
Average crystallite size = 25.0 nm				

peak broadening and crystallite size was calculated using full width at half-maximum (FWHM) values and Scherrer's equation.

The nanoparticles synthesized in this study demonstrated minimal Δd_{hkl} values, approximately 10^{-3} nm, indicating a close match between the observed *d*-spacing of the diffraction planes and the standard values. The deviation in *d*-spacing, which measures the displacement of diffraction lines, is an indicator of the microstrain present in the nanopowder sample. To determine the microstrain in the particles along the direction normal to the diffraction plane, the observed *d*-spacing (d_0) of the prepared sample is compared to the spacing in the standard sample (d_s). If $d_0 > d_s$, it indicates a positive microstrain, suggesting the presence of residual tensile stress. Conversely, if $d_0 < d_s$, it signifies a negative micro-strain, indicating the generation of residual compressive stress on the surface. This comparison provides valuable insights into the magnitude and nature of the residual stresses within the synthesized nanoparticles was determined as Δd_{hkl}. If $d_0 > d_s$, a positive micro-strain indicated the presence of residual tensile stress. Conversely, if $d_0 < d_s$, a negative micro-strain indicated the generation of residual compressive stress on the surface. These findings offer valuable insights into the nature and magnitude of the residual stresses present within the synthesized nanoparticles.

FTIR studies: In the case of ZnO nanoparticles, the peak at 484 cm^{-1} corresponds to the characteristic stretching vibration of Zn-O bonds, which are the primary bonds in the ZnO crystal lattice. The peak at 3400 cm^{-1} represents the broad stretching vibration of hydroxyl groups (O-H) or adsorbed water molecules (H-O-H). It indicates the presence of surface hydroxyl groups or moisture absorbed on the surface of ZnO nanoparticles. The peak at 1626 cm^{-1} is typically associated with the stretching vibration of adsorbed water molecules (H-O-H). It further supports the presence of water on the surface of the nanoparticles. The peaks in the range of 1649-1400 cm^{-1} encompass several possible vibrational modes. It could be attributed to the presence of carboxylic acids (-COOH) or carbonyl groups (-C=O) indicating the presence of organic species or functional groups on the surface of ZnO nanoparticles. The peak at 2424 cm^{-1} suggests the presence of carbon dioxide (CO_2) or carbonate species (CO_3^{2-}) adsorbed on the surface of ZnO nanoparticles. It may indicate the interaction of ZnO nanoparticles with atmospheric carbon dioxide or the presence of carbonate impurities in the sample (Fig. 2). Overall, the observed FTIR peaks provide valuable insights into the surface chemistry of ZnO nanoparticles. The peaks associated with Zn-O bonds confirm the presence of ZnO nanoparticles, while the peaks related to hydroxyl groups, adsorbed water molecules, organic species and carbonate species indicate the presence of surface functional groups and potential impurities. The FTIR analysis serves as a useful tool for understanding the surface properties and potential applications of ZnO nanoparticles [12].

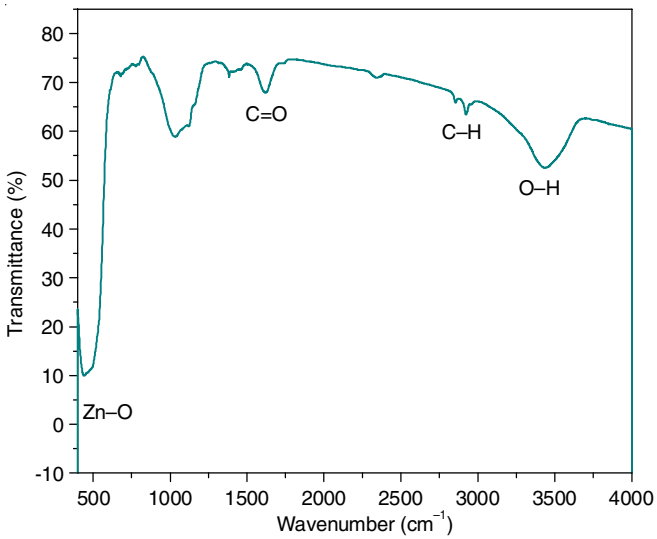

Fig. 2. FT-IR spectra of ZnO nanoparticles

UV-DRS studies: In case of ZnO nanoparticles with a band gap of 3.35 eV, the UV-DRS studies provide valuable information about their light absorption and electronic transitions. In UV-DRS, the material is illuminated with a broad range of UV and visible light wavelengths and the amount of light reflected was measured. The absorption spectrum obtained from UV-DRS analysis can be used to determine the band gap energy of the material. The ZnO nanoparticles with a band gap of 3.35 eV would exhibit strong absorption in the UV region, extending into the visible range. The absorption edge, which corresponds to the onset of significant absorption, would be observed at a wavelength corresponding to the band gap energy. In the UV-DRS spectrum of ZnO nanoparticles, a sharp increase in absorption would be observed in the UV region, typically below 400 nm. This strong absorption is attributed to the direct band gap transition in ZnO nanoparticles, where electrons are excited from the valence band to the conduction band. The band gap energy of 3.35 eV indicates that ZnO nanoparticles can efficiently absorb light in the UV region and a portion of the visible region. This makes them suitable for various applications such as photocatalysis, UV sensors and optoelectronic devices. UV-DRS studies provide quantitative information about the optical properties of ZnO nanoparticles, including their band gap energy. This information is crucial for understanding the light absorption and electronic transitions occurring in the material, enabling researchers to optimize its performance for specific applications. The diffused reflectance was calculated by Kubelka-Munk function F(R):

$$F(R) = \frac{(1-R)^2}{2R} \quad (3)$$

where R represents the reflectance.

The Kubelka-Munk function enables the characterization of the powders based on their reflectance properties, providing the valuable insights into the absorption coefficient and optical behavior of the ZnO nanoparticles.

By utilizing Tauc relation the optical energy bandgap of the synthesized material was determined [13] and the relation is given in eqn. 4:

$$F(R)\ h\nu = A\ (h\nu - E_g)^n \quad (4)$$

where for direct and for indirect transitions n values were taken as ½ and 2.

The synthesized ZnO nanoparticles exhibited a calculated energy band gap of 3.35 eV, as illustrated in Fig. 3. The energy band gap of a material significantly influences its catalytic performance. A highly efficient photocatalyst demonstrates a broad absorption range encompassing both the UV and visible spectra. As the size of the material decreases, the quantum confinement effect becomes more prominent. This effect leads to the generation of a higher number of electron-hole pairs, ultimately enhancing the photocatalytic efficiency of the material [13].

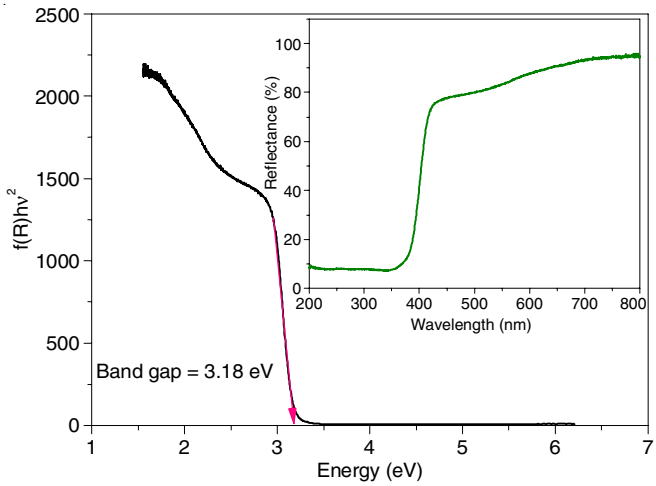

Fig. 3. Diffuseareflectance spectra (inset) and energy gap spectra of ZnO nanoparticles

Morphological studies: Significant insights into the morphological characteristics of the ZnO nanoparticles have been obtained through the effective utilization of TEM micrographs and patterns. Fig. 4a-b illustrates the TEM images, HRTEM and SAED patterns of the as-synthesized ZnO nanoparticles, revealing their predominantly spherical shape, although both

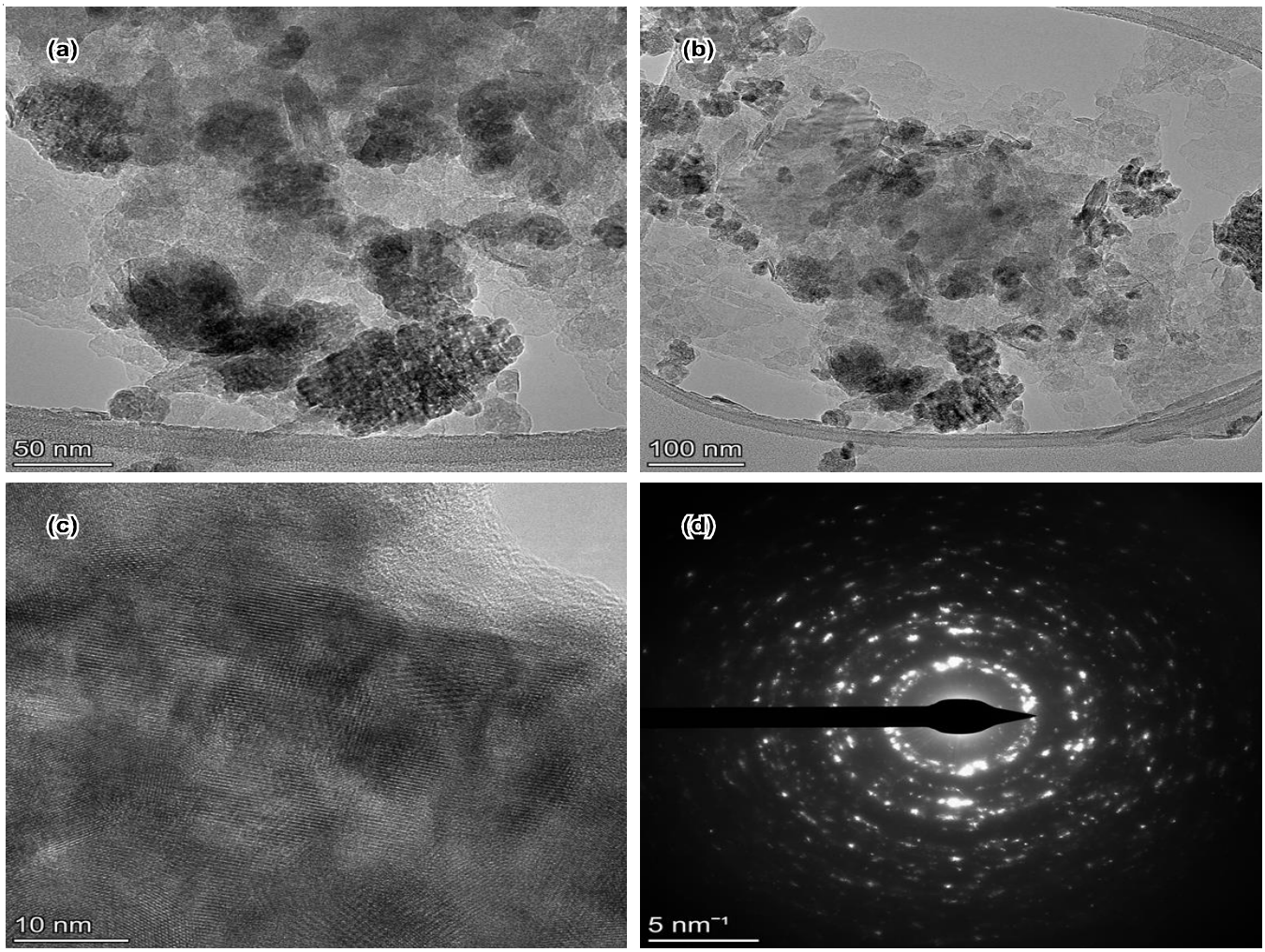

Fig. 4. (a&b) TEM images, (c) HRTEM and (d) SAED pattern of ZnO NPs

regular and asymmetric geometries are observed. The presence of nanoparticles with sizes ranging from 25 to 30 nm, or even smaller, indicates the efficiency of the probe sonication method employed during synthesis. This efficient sonication prevented the formation of agglomerated particles, ensuring the formation of well-dispersed individual nanoparticles [14].

Photocatalytic studies: In the dye decolorization experiments, a circular glass reactor with a surface area of 176.6 cm^2 was utilized. The reactor contained a 125 W medium-pressure mercury vapor lamp, which served as the UV light source. Each experimental run involved the dispersion of approximately 60 mg of photocatalyst into a 250 mL solution containing 20 ppm of dye. The photocatalyst was evenly distributed within the solution, ensuring optimal contact between the catalyst and the dye molecules. To initiate the photocatalytic reaction, the reaction mixture was subjected to direct irradiation by placing the lamp at a distance of 23 cm from the reactor. This distance was chosen to optimize the light intensity reaching the reaction mixture. The medium-pressure mercury vapour lamp emitted UV light, which is known to activate the photocatalyst and facilitate the degradation process. Throughout the experiment, a magnetic stirrer was employed to ensure proper mixing of the reaction mixture. Vigorous stirring helped to maintain a homogeneous distribution of the dye and photocatalyst, enhancing the contact between the two and promoting efficient degradation. The extent of adsorption (Q) was determined using the following eqn 3:

$$Q = \frac{(C_o - C)V}{W} \quad (5)$$

where C_o and C represent the concentrations of dye solution before and after adsorption, respectively; V denotes the volume of reaction mixture and W represents the weight of catalyst (g).

During the course of the experiment, samples of 5 mL were withdrawn at regular intervals from the suspensions. These samples were immediately centrifuged and filtered through a Whatman filter paper to remove any catalyst particles. Subsequently, the filtered solution was subjected to spectrophotometric analysis to determine the concentration of dye remaining in the solution.

Decolourization of direct green (DG) dye: Fig. 5a-b illustrates the outcomes of the photocatalytic studies conducted using ZnO nanoparticles prepared using the probe sonication method, as evaluated through the photo-decolourization of direct green dye under sunlight and UV light irradiation. The Fig. 5a indicates that ZnO nanoparticles demonstrates significant photocatalytic activity, attributed to the rapid recombination of photogenerated electrons and holes [15]. The sample exhibited a decolorization efficiency of 66.07% after 120 min of UV light irradiation, indicating its effective dye degradation capabilities. However, under sunlight irradiation, ZnO showed a slightly lower efficiency, achieving 67.93% dye degradation within the same 120 min timeframe. These results highlighted the photocatalytic potential of ZnO nanoparticles indicating their ability to degrade direct green dye effectively, particularly under UV light irradiation.

Table-2 shows the UV-visible spectral analysis results of the decolourization kinetics of the direct green dye at different time intervals (ranging from 0 to 120 min) at a specific wavelength of 620 nm. The data clearly illustrates a consistent decrease in the direct green dye concentrations over time when ZnO nanoparticles are present. This indicates a significant reduction in the colour intensity of the dye under both sunlight and UV light irradiation. To further analyze the decolorization process, logarithm values of C/C_o were calculated using eqn. 6, where C_o and C represent the dye concentration at t = 0 min and the respective testing time and k is the first-order rate constant. From the results obtained, it is clear that the reaction follows first-order kinetics as the results showcase that relationship between the log (C/C_o) and k is linear. The slope values for ZnO nanoparticles synthesized by the green and chemical methods were determined as 0.020155 min^{-1} and 0.0101502 min^{-1}, respectively. The dye degradation of direct green and fast orange dyes was calculated using the concentration of dye remaining during photocatalysis by the following equation:

$$\text{Degradation } (\%) = \frac{C_o - C}{C} \times 100 \quad (4)$$

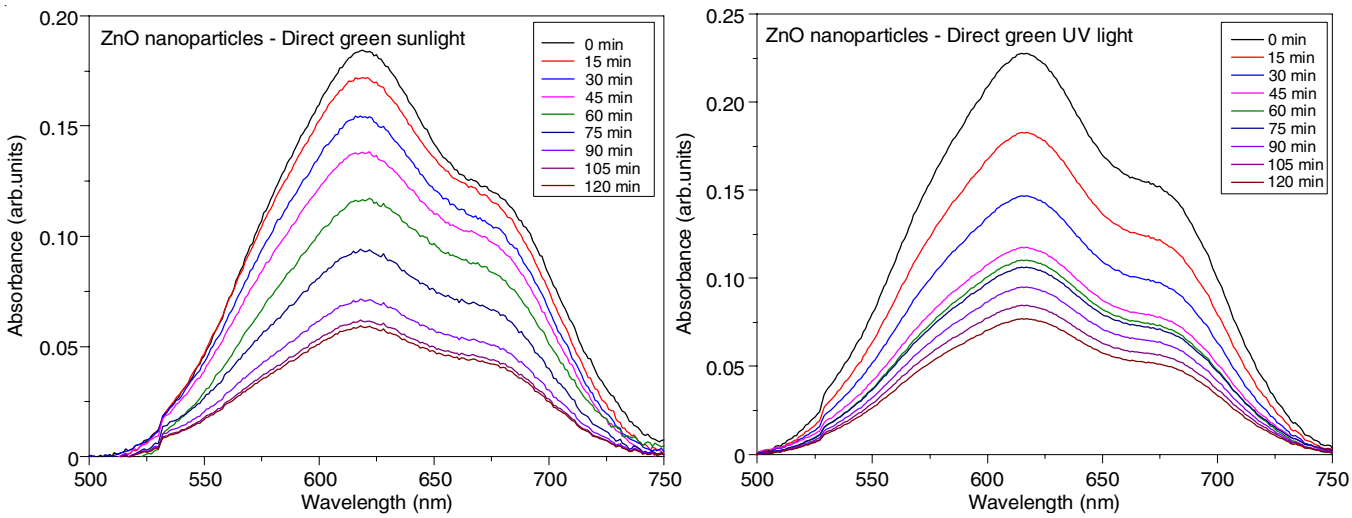

Fig. 5. (a&b) UV-Vis absorbance spectra of direct green (DG) for ZnO NPs synthesized by probe sonication method under sunlight and UV light irradiation

TABLE-2
RATE CONSTANTS AND KINETIC STUDIES OF ZnO NANOPARTICLES SYNTHESIZED FOR THE DECOLORIZATION OF DIRECT GREEN (DG) UNDER UV LIGHT

t	20 ppm Direct green + 60 mg ZnO + sunlight					20 ppm Direct green + 60 mg ZnO + UV				
	C	C/C_o	log C/C_o	-log C/C_o	D (%)	C	C/C_o	log C/C_o	-log C/C_o	D (%)
0	0.184	1	0	0	0	0.227	1	0	0	0
15	0.172	0.934	-0.0296	0.0296	6.52	0.183	0.806	-0.0936	0.0936	19.38
30	0.154	0.836	-0.0777	0.0777	16.30	0.147	0.647	-0.1890	0.1890	35.24
45	0.138	0.750	-0.1249	0.1249	25.00	0.117	0.515	-0.2881	0.2881	48.45
60	0.116	0.630	-0.2006	0.2006	36.95	0.110	0.484	-0.3151	-0.3151	51.54
75	0.093	0.505	-0.2967	0.2967	49.45	0.106	0.466	-0.3316	-0.3316	53.30
90	0.071	0.385	-0.4145	0.4145	61.41	0.094	0.414	-0.3829	-0.3829	58.59
105	0.062	0.336	-0.4736	0.4736	66.30	0.085	0.374	-0.4271	-0.4271	62.55
120	0.059	0.320	-0.4948	0.4948	67.93	0.077	0.339	-0.4698	-0.4698	66.07

Furthermore, the photocatalytic decolorization efficiency (% D) of the direct green dye was determined using eqn. 7, where (% D) represents the efficiency of photo-decolorization, the initial concentration of the dye solution is denoted as C_o, while the concentration of dye after a specific time is represented as C. The below given mechanism is a general explanation for the degradation of direct green dye by the synthesized ZnO nanoparticles.

$$ZnO + UV\ light \longrightarrow e^- + h^+ \quad (8)$$

$$h^+ + H_2O \longrightarrow OH^\bullet + H^+ \quad (9)$$

$$O_2 + e^- \longrightarrow O_2^{\bullet-} \quad (10)$$

$$O_2^{\bullet-} + H^+ \longrightarrow OOH^\bullet \quad (11)$$

$$ZnO + O_2^{\bullet-} + 2H^+ \longrightarrow ZnO + H_2O_2 \quad (12)$$

$$ZnO(e^-) + H_2O_2 + e^- \longrightarrow ZnO + OH^\bullet + OH^- \quad (13)$$

$$Dye + (O_2 + O_2^{\bullet-} + OOH^\bullet) \longrightarrow Decolorization\ product \quad (14)$$

The efficient decolorization of dyes and organic pollutants in wastewater into less harmful compounds such as CO_2 and H_2O is primarily attributed to the presence of active oxygen species (O_2, $O_2^{\bullet-}$) and hydroxyl free radicals. In this context, photocatalytic studies have revealed that ZnO nanoparticles prepared using the probe sonication method exhibit notable effectiveness in the decolorization of direct green dye. These ZnO nanoparticle demonstrate a strong ability to generate the necessary active oxygen species and hydroxyl free radicals, which are crucial for the degradation of dyes and organic contaminants, leading to their transformation into environmentally benign substances [16].

Decolourization of fast orange dye: The photocatalytic decolourization effectiveness of fast orange dye was also investigated using ZnO nanoparticles prepared *via* the probe sonication method under both sunlight and UV light irradiation. The rate of decolorization of the dye particles was evaluated based on the catalyst mass and concentration used. Fig. 6a-b depicts the absorption peak of fast orange dye at 610 nm under sunlight and 510 nm under UV light irradiation, showing a gradual decrease over time (from 0 to 120 min), indicating the photo-decolorization capability of ZnO nanoparticles.

Table-3 presents a summary of the kinetic parameters and percentage degradation obtained from the experimental data. The results indicate that ZnO nanoparticles prepared by the probe sonication method exhibited a fast orange dye decolorization efficiency of 67.93% and 94.66% under sunlight and UV light irradiation, respectively, after a 120 min irradiation time. These findings highlight the promising photocatalytic

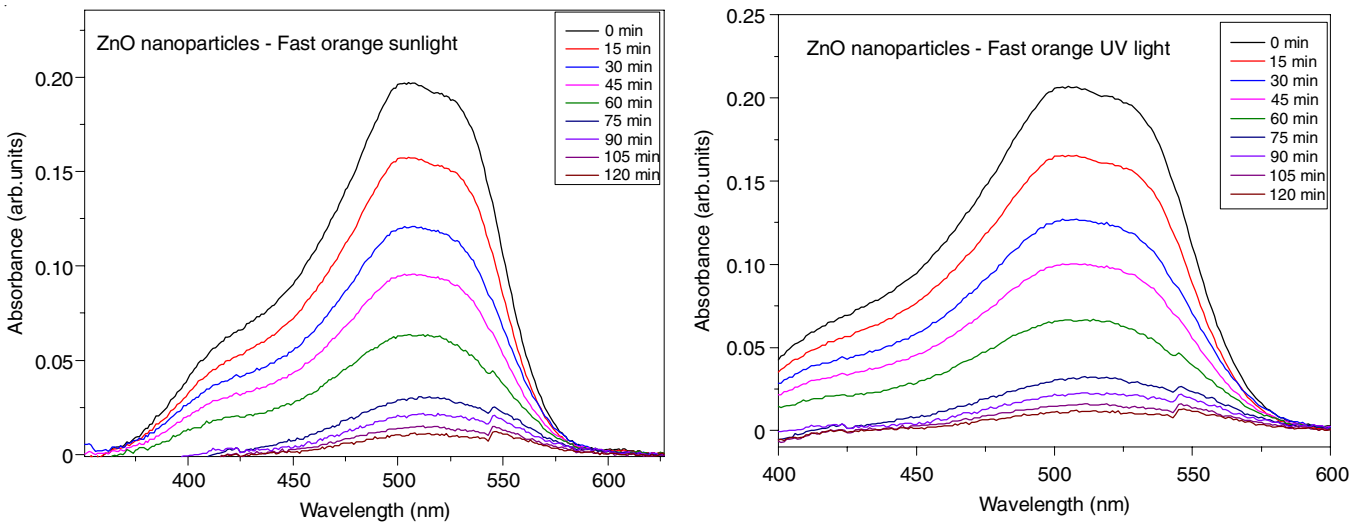

Fig. 6. (a&b) Absorbance spectra of fast orange (FO) for ZnO nanoparticles synthesized by probe sonication method under sunlight and UV light irradiation

TABLE-3
RATE CONSTANTS AND KINETIC STUDIES OF ZnO NANOPARTICLES SYNTHESIZED BY PROBE SONICATION METHOD FOR THE DECOLORIZATION OF FAST ORANGE (FO) UNDER SUNLIGHT AND UV LIGHT

t	20 ppm Fast orange + 60 mg ZnO + sunlight					20 ppm Fast orange + 60 mg ZnO + UV				
	C	C/C_o	log C/C_o	-log C/C_o	D (%)	C	C/C_o	log C/C_o	-log C/C_o	D (%)
0	0.184	1	0	0	0	0.206	1	0	0	0
15	0.171	0.929	-0.0319	0.0319	7.06	0.166	0.805	-0.0942	0.0942	19.41
30	0.154	0.836	-0.0777	0.0777	16.30	0.127	0.616	-0.2104	0.2104	38.34
45	0.137	0.744	-0.1284	0.1284	25.54	0.100	0.485	-0.3142	0.3142	51.45
60	0.117	0.635	-0.1972	0.1972	36.41	0.065	0.315	-0.5016	0.5016	68.44
75	0.092	0.500	-0.3010	0.3010	50.00	0.032	0.155	-0.8096	0.8096	84.46
90	0.072	0.391	-0.4078	0.4078	60.86	0.021	0.109	-0.9956	0.9956	89.80
105	0.062	0.336	-0.4736	0.4736	66.30	0.017	0.082	-1.0861	1.0861	91.74
120	0.059	0.320	-0.4948	0.4948	67.93	0.011	0.053	-1.2757	1.2757	94.66

performance of ZnO nanoparticles in the degradation of fast orange dye, with higher degradation rates observed under UV light compared to sunlight.

Here, the degradation kinetics of fast orange dye follows pseudo-first order kinetics and the results are shown in Table-3, which also aligns with the Langmuir-Hinshelwood model. This model suggests that the reaction rate is proportional to the concentration of dye and the active sites on ZnO nanoparticles' surface. Furthermore, the UV-Visible absorption spectra provide evidence of a greater extent of photocatalytic degradation of the dye when ZnO nanoparticles were employed under UV light irradiation. The absorption spectra demonstrate a significant reduction in the dye's concentration, indicating the effectiveness of ZnO nanoparticles as photocatalysts in promoting the degradation process.

The enhanced photocatalytic activity observed under UV light irradiation can be attributed to the following factors: (a) the use of UV light has sufficient energy to excite electrons from the valence band to the conduction band of ZnO, creating electron-hole pairs. UV light consists of higher energy photons compared to visible light, which leads to increased excitation of electrons from the valence band to the conduction band of the ZnO NPs. This promotes the generation and transportation of electron-hole pairs, which are vital for the degradation of the dye molecules; (b) the catalyst has higher absorptive capacity for the fast orange dye, since the π–π interaction between ZnO and the fast orange dye molecules leads to a stronger adsorption of the dye onto the catalyst surface under UV light irradiation. This improved adsorption facilitates efficient contact between the dye and the active sites on the ZnO nanoparticles, enhancing the photocatalytic degradation process. Taken together, these factors contribute to the higher photocatalytic activity exhibited by ZnO nanoparticles under UV light irradiation, resulting in increased efficiency and degradation of the fast orange dye molecules [17,18].

Electrochemical sensor studies: The electrochemical studies were performed using a three-electrode system, where the working electrode consisted of a composite material composed of 70% graphite, 15% ZnO nanoparticles and 15% silicon oil. This composite material served as the working electrode for the cyclic voltammetric measurements. During the cyclic voltammetric studies, the voltage range of -0.4 V to +0.6 V was applied to the working electrode. Within this range, the oxidation and reduction potentials associated with the ZnO nanoparticles were determined. The oxidation potential for the ZnO nanoparticles was found to be 0.64 V, indicating the voltage at which the oxidation reaction occurs on the surface of the working electrode. This potential represents the energy required to remove electrons from the ZnO nanoparticles, resulting in the formation of oxidized species. Similarly, the reduction potential for the ZnO nanoparticles was determined to be 0.39 V. This potential corresponds to the voltage at which the reduction reaction takes place on the working electrode. It represents the energy required to add electrons to the ZnO nanoparticles, leading to the formation of reduced species.

The CV curves for the ZnO nanoparticles is presented in Fig. 7. It is important to note that the observed capacitance in the CV curve does not exhibit the typical rectangular shape associated with an electrical double-layer capacitor [19]. Instead, the curve indicates a different behaviour attributed to a redox mechanism. The CV curve shows an anodic peak, which corresponds to the oxidation of ZnO nanoparticles into Zn^{2+} ions. Conversely, the cathodic peak represents the reduction of Zn^{2+} ions back to ZnO nanoparticles. The observation of a quasi-reversible electron transfer process indicates that the electron transfer reaction in question occurs with some degree of reversibility. In other words, while the electron transfer is not completely reversible, it is not entirely irreversible either occurring during the oxidation and reduction reactions [20]. In a CV measurement, the applied potential was varied cyclically and the resulting current response was recorded. The potential difference ($E_O - E_R$) between the oxidation and reduction potentials determines the overall direction of the redox reaction. If the potential difference is positive ($E_O > E_R$), the reaction is more favourable for oxidation and electrons flow from the species with the lower oxidation potential to the species with the higher reduction potential. Conversely, if the potential difference is negative ($E_O < E_R$), the reaction is more favourable for reduction and electrons flow from the species with the higher oxidation potential to the species with the lower reduction potential. A smaller difference suggests a higher degree of reversibility [21]. In case of ZnO electrodes, it is evident that the difference between the oxidation and reduction peaks is greater for the sample prepared using the sonochemical method. The calculated values for E_O and E_R were found to be 0.6414 V and 0.3941 V, respectively (Fig. 7). When the difference between

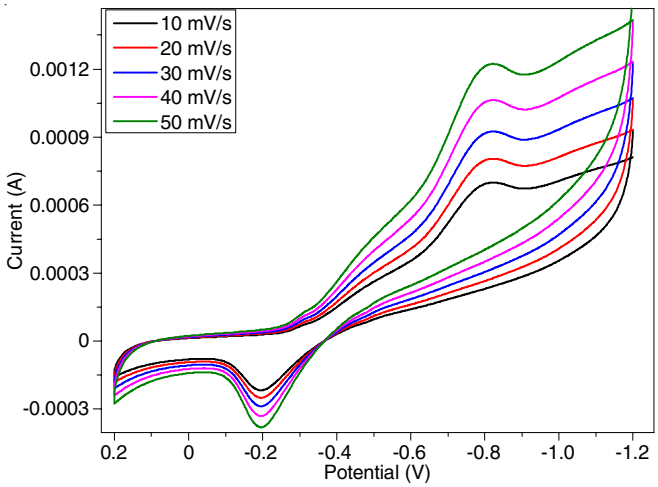

Fig. 7. Cyclic voltammogram of ZnO electrode at different scan rate V/s Ag/AgCl electrode

E_O and E_R is smaller, the evolution of oxygen during the oxidation process becomes easier. This leads to increased charge efficiency, improved utilization of the active material and higher reversibility of the electrochemical reaction of the electrode [22].

The stable state of the electrochemical impedance measurements were measured using Ag/AgCl electrode in the frequency range of 1 Hz to 1 MHz with 5 mV AC amplitude. The Nyquist plots of different ZnO electrodes are shown in Fig. 8.

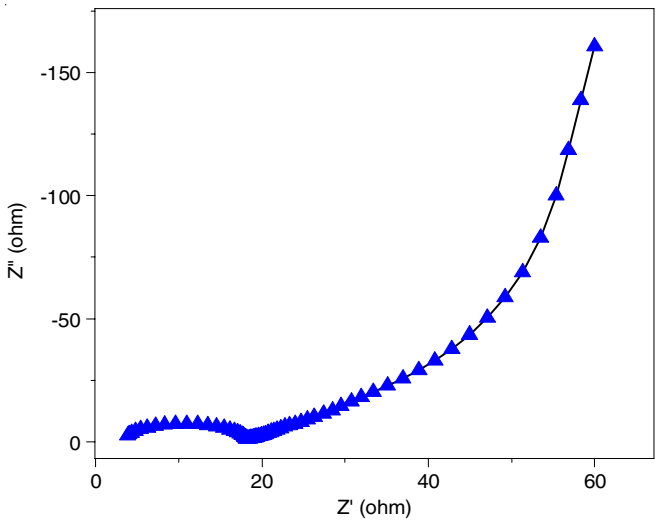

Fig. 8. Nyquist plot of ZnO NPs electrode

The overall impedance (Z) of the prepared electrode can be expressed as:

$$Z(w) = Z' + jZ'' = Z_{Re} + jZ_{Im} = R + j\,X \quad (14)$$

$$j = \sqrt{-1} \quad (15)$$

where Z′ or Z_{Re} and Z″ or Z_{Im} were the real and imaginary parts of the impedance [23].

The impedance spectra of the ZnO electrode exhibit larger impedance values, indicating increased resistance to the flow of electric current. This higher impedance can be attributed to several factors, including the presence of ZnO layer and the electrochemical processes occurring at the electrode-electrolyte interface.

When a depressed semicircle is observed in the high-frequency region of the EIS spectrum, it suggests the presence of a capacitive element in the system. By incorporating the constant phase element (Q1) into the equivalent circuit, a more accurate representation of the electrochemical system can be achieved, allowing for a better fit of the experimental data obtained from techniques such as electrochemical impedance spectroscopy (EIS).

$$Z_{CPE} = \frac{1}{Y(j\omega)^n} \quad (16)$$

In the equation, ω represents the angular frequency in rad s^{-1} and Y and n are adjustable parameters associated with the constant phase element (Q1). The value of n in the constant phase element (Q1) can indeed take on the values of 1, 0 or 0.5, corresponding to different electrochemical phenomena: when n = 1, it represents the double-layer capacitance (Cdl). When n = 0, it represents the resistance (R) of the system. When n = 0.5, it represents the Warburg diffusion (W) behaviour.

The Nyquist plots of impedance measurements for different ZnO electrodes are represented by the equivalent circuit shown in Fig. 9. In this circuit, the high-frequency region intercepting the semicircle on the real axis of the Nyquist spectrum corresponds to the solution resistance (R_s), which indicates resistance at the electrode-electrolyte interface. The semicircles observed in the plot are attributed to either interfacial charge transfer resistance (R_{ct}) or polarization resistance (R_p), which are connected in parallel to the double-layer capacitance (C). Overall, the observation of a straight line in the low-frequency region of the Nyquist plot indicates the presence of a Warburg element, emphasizing the importance of diffusion processes in the electrochemical system being studied. The observation of a straight line in the low-frequency region of the Nyquist plot suggests that the diffusion of zinc ions and electrons into the pores on the surface of the ZnO electrodes plays a significant role in the electrochemical behaviour of the system [14]. The semicircle shape arises due to the interplay between the capacitive behavior of the electrical double layer and the resistive behavior of the charge transfer process. The diameter of the semicircle is related to the charge transfer resistance (R_{ct}) with larger semicircles corresponding to higher resistance values. Within the equivalent circuit, the constant phase element (Q) is placed

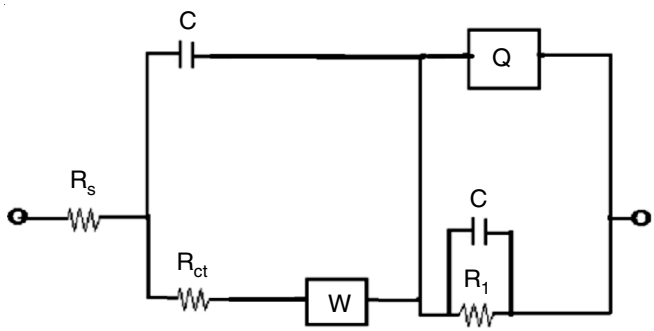

Fig. 9. Equivalent circuit of the Nyquist plots of an impedance measurement of different ZnO electrode

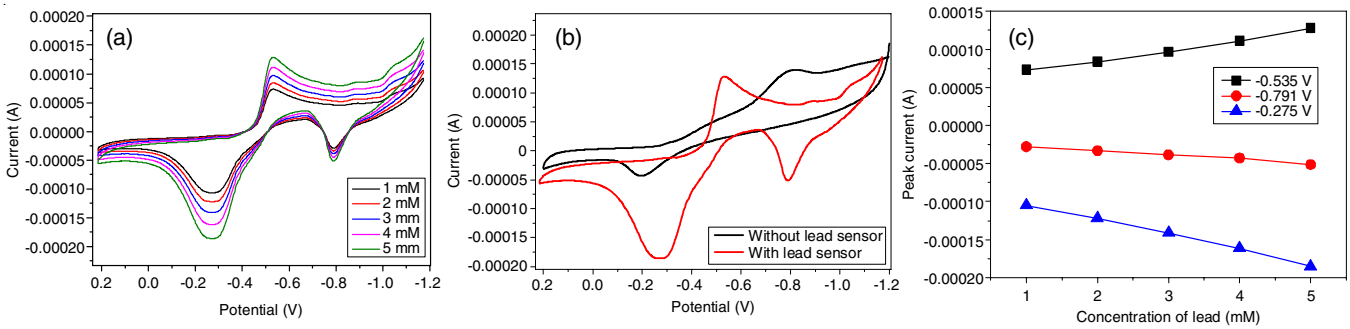

Fig. 10. (a) Cyclic voltammogram of ZnO electrode during detection of lead, concentration range 1-5 mM, (b) cyclic voltammogram of CPE electrode ZnO electrode with and without lead sensor and (c) peak current *vs.* concentration of lead

in parallel with the charge-transfer resistance (R_{ct}) and the leakage resistance (Rl) [23].

The ZnO nanoparticles used to detect lead (Pb) have cyclic voltammograms, which are shown in Fig. 10a. A sharp shift in the locations of the oxidation and reduction peaks suggests that the ZnO nanoparticles used to make the carbon paste electrode are appropriate for use as sensors in acidic media at concentrations of 1 to 5 mM. Additionally, the current response grows with additional injections of 1 mM lead over 50s of sampling time, reaching steady state in under 3s. The anodic oxidation and reduction peaks on the ZnO electrode are at -0.2 V and -0.815 V, respectively (Fig. 10b). On the anodic and cathodic sides of the lead sensor, there are additional peaks on the cyclic voltammogram, with oxidation peaks at -0.535 and -0.791 V and reduction peak shifted to at -0.275 V. The CV of the ZnO electrode in the presence and absence of a lead sensor is shown in Fig. 10b, confirming that the peak positions clearly change when lead is added to the electrolyte.

Fig. 10c, shows the anodic and cathodic current responses in relation to lead concentration. The ZnO electrode sensor exhibits an approximately linear trend in with decrease in anodic current at both potentials, but a rise in cathodic current at -0.275 V as lead concentration was increased. This further highlights the exceptional sensitivity of the ZnO modified electrode to the electrochemical activity of the heavy metal under study.

Conclusion

In summary, ZnO nanoparticles were successfully synthesized through the sonochemical route and their crystallinity was confirmed using XRD analysis. Optical studies revealed that the synthesized ZnO nanoparticles possess a bandgap of 3.35 eV. Morphological investigations demonstrated that the nanoparticles were well-dispersed and exhibited a crystalline structure. The catalytic applications of these synthesized nanomaterials were examined by employing them for the degradation of direct green and fast orange dyes under both visible and UV light conditions. Remarkably, the ZnO nanoparticles exhibited excellent catalytic properties, achieving a degradation efficiency of 94.6% for fast orange dyes within 120 min. Moreover, electrocatalytic studies demonstrated a redox reaction, indicating that the material is suitable for both photocatalysis and electrochemical lead sensor.

CONFLICT OF INTEREST

The authors declare that there is no conflict of interests regarding the publication of this article.

REFERENCES

1. S. Sabir, M. Arshad and S.K. Chaudhari, *Scient. World J.*, **2014**, 925494 (2014); https://doi.org/10.1155/2014/925494
2. M. Arakha, S. Pal, D. Samantarrai, T.K. Panigrahi, B.C. Mallick, K. Pramanik, B. Mallick and S. Jha, *Sci. Rep.*, **5**, 14813 (2015); https://doi.org/10.1038/srep14813
3. X. Bai, L. Li, H. Liu, L. Tan, T. Liu and X. Meng, *ACS Appl. Mater. Interfaces*, **7**, 1308 (2015); https://doi.org/10.1021/am507532p
4. U. Ozgür, Y.I. Alivov, C. Liu, A. Teke, M.A. Reshchikov, S. Doğan, V. Avrutin, S.-J. Cho and H. Morkoç, *J. Appl. Phys.*, **98**, 041301 (2005); https://doi.org/10.1063/1.1992666
5. M. Moritz and M. Geszke-Moritz, *Chem. Eng. J.*, **228**, 596 (2013); https://doi.org/10.1016/j.cej.2013.05.046
6. A.A. Reinert, C. Payne, L. Wang, J. Ciston, Y. Zhu and P.G. Khalifah, *Inorg. Chem.*, **52**, 8389 (2013); https://doi.org/10.1021/ic400011n.
7. B. Ludi and M. Niederberger, *Dalton Trans.*, **42**, 12554 (2013); https://doi.org/10.1039/c3dt50610j
8. B. Kumar, K. Smita, L. Cumbal and A. Debut, *Bioinorg. Chem. Appl.*, **2014**, 784268 (2014); https://doi.org/10.1155/2014/784268
9. G.R. Navyashree, H. Nagabhushana, D.V. Sunitha and S. Yeshodamma, *Int. J. Eng. Res.*, **I**, 790 (2016).
10. S.Y. Pung, C.S. Ong, K.M. Isha and M.H. Othman, *Sains Malays.*, **43**, 273 (2014).
11. R. Suntako, *Bull. Mater. Sci.*, **38**, 1033 (2015); https://doi.org/10.1007/s12034-015-0921-0
12. A.P. Zhang and J.Z. Zhang, *J. Alloys Compd.*, **491**, 631 (2010); https://doi.org/10.1016/j.jallcom.2009.11.027
13. T. Takizawa, T. Watanabe and K. Honda, *J. Phys. Chem.*, **82**, 1391 (1978); https://doi.org/10.1021/j100501a014
14. P. Nithyadharseni, K.P. Abhilash, S. Petnikota, M.R. Anilkumar, R. Jose, K.I. Ozoemena, R. Vijayaraghavan, P. Kulkarni, G. Balakrishna, B.V.R. Chowdari, S. Adams and M.V. Reddy, *Electrochim. Acta*, **247**, 358 (2017); https://doi.org/10.1016/j.electacta.2017.06.170
15. V.N. Kalpana and V.D. Rajeswari, *Bioinorg. Chem. Appl.*, **2018**, 3569758 (2018); https://doi.org/10.1155/2018/3569758
16. J. Yang, X. Zhao, X. Shan, H. Fan, L. Yang, Y. Zhang and X. Li, *J. Alloys Compd.*, **556**, 1 (2013); https://doi.org/10.1016/j.jallcom.2012.12.098

17. J.J. Xu, Y.H. Ao, D.G. Fu and C.W. Yuan, *J. Hazard. Mater.*, **164**, 762 (2009); https://doi.org/10.1016/j.jhazmat.2008.08.108
18. J.A. Anta, E. Guillén and R. Tena-Zaera, *J. Phys. Chem. C*, **116**, 11413 (2012); https://doi.org/10.1021/jp3010025
19. C.R. Ravikumar, M.S. Santosh, H.P. Nagaswarupa, S.C. Prashantha, S. Yallappa and M.R. Anil Kumar, *Mater. Res. Express*, **4**, 065503 (2017); https://doi.org/10.1088/2053-1591/aa73a5
20. C.R. Ravi kumar, P. Kotteeswaran, V.B. Raju, A. Murugan, M.S. Santosh, H.P. Nagaswarupa, S.C. Prashantha, M.R.A. Kumar and M.S. Shivakumar, *J. Energy Storage*, **9**, 12 (2017); https://doi.org/10.1016/j.est.2016.11.001
21. K.M. Girish, S.C. Prashantha, H. Nagabhushana, C.R. Ravikumar, H.P. Nagaswarupa, R. Naik, H.B. Premakumar and B. Umesh, *J. Sci. Adv. Mater. Devices*, **3**, 151 (2018); https://doi.org/10.1016/j.jsamd.2018.02.001
22. C.R. Ravikumar, M.R.A. Kumar, H.P. Nagaswarupa, S.C. Prashantha, A.S. Bhatt, M.S. Santosh and D. Kuznetsov, *J. Alloys Compd.*, **736**, 332 (2018); https://doi.org/10.1016/j.jallcom.2017.11.111
23. D. Darbar, M.R. Anilkumar, V. Rajagopalan and I. Bhattacharya, *Ceramic Int.*, **44**, 4630 (2017); https://doi.org/10.1016/j.ceramint.2017.12.010